JOURNAL OF MATERIALS SCIENCE **34** (1999) 5757–5769

# The displacive compensation of porosity (DCP) method for fabricating dense, shaped, high-ceramic-bearing bodies at modest temperatures

P. KUMAR, K. H. SANDHAGE
*Department of Materials Science and Engineering, 477 Watts Hall, 116 W. 19th Avenue, The Ohio State University, Columbus, OH 43210 USA*
*E-mail: sandhage@KCGL1.eng.ohio-state.edu*

A novel process is introduced for the fabrication of dense, shaped ceramic/metal composites of high ceramic content: the Displacive Compensation of Porosity (DCP) method. In this process, a metallic liquid is allowed to infiltrate and undergo a displacement reaction with a porous oxide preform. Unlike other displacement-reaction-based processes (e.g., the $C^4$, RMP, and AAA processes), a larger volume of oxide is generated than is consumed, so that composites with relatively high ceramic contents can be fabricated. Bar- and disk-shaped MgO/Mg-Al composites were produced by the infiltration and reaction of molten Mg with porous $Al_2O_3$ preforms at 1000 °C. By varying the relative density of the preforms (from 53.3 to 71.0% of theoretical), the magnesia content of the final composites could be adjusted from 70.4 to 85.6 vol %. Because the increase in oxide volume associated with the conversion of alumina into magnesia was accommodated by the prior pore volume of the preforms, the composites retained the shapes and dimensions (to within a few percent) of the starting preforms. The MgO/Mg-Al composites were lightweight (2.94–3.30 g/cm$^3$), dense (97.7–99.0% of theoretical), and resistant to hydration. Bar-shaped MgO/Mg-Al composites exhibited average flexural strength and indentation toughness values of 244 MPa and 5.4 MPa · m$^{1/2}$, respectively. 

## 1. Introduction

Several displacement-reaction-based processing routes involving reactive metallic liquids have recently been developed to produce bulk, shaped ceramic/metal composites [1–10]. In the Co-Continuous Ceramic Composite ($C^4$) process [1, 2], $Al_2O_3$/Al(Si) composites have been produced by allowing liquid aluminum to undergo a displacement reaction with shaped, solid, amorphous silica preforms at ≥1000 °C, as per the following net reaction:

$$4\{Al\} + 3SiO_2 = 2Al_2O_3 + 3\{Si\} \quad (1a)$$

where the brackets { } denote a species dissolved in a liquid solution. In the Alumina Aluminide Alloy (AAA) [3–5] and Reactive Metal Penetration (RMP) [6–10] processes, liquid aluminum is allowed to react with crystalline oxides (silica, mullite, titania, etc.) to produce composites of $Al_2O_3$ with Al-bearing metal alloys or intermetallic compounds, as indicated by reactions of the following type:

$$(8 + 6x)\{Al\} + 3Al_6Si_2O_{13} = 13Al_2O_3(s) + 6\{SiAl_x\} \quad (1b)$$

$$(4 + 3x)\{Al\} + 3TiO_2 = 2Al_2O_3(s) + 3TiAl_x \quad (1c)$$

$$(4 + 3x)\{Al\} + 3Al_2TiO_5 = 5Al_2O_3(s) + 3TiAl_x \quad (1d)$$

$$(2 + 3x)\{Al\} + 3NiO = Al_2O_3(s) + 3NiAl_x \quad (1e)$$

$$(2 + 3x)\{Al\} + 3NiAl_2O_4 = 4Al_2O_3(s) + 3NiAl_x \quad (1f)$$

$$(10 + 6x)\{Al\} + 3Nb_2O_5 = 5Al_2O_3(s) + 6NbAl_x \quad (1g)$$

$$(4 + 3x)\{Al\} + 3ZrO_2 = 2Al_2O_3(s) + 3ZrAl_x \quad (1h)$$

$$(8 + 9x)\{Al\} + 3Fe_3O_4 = 4Al_2O_3(s) + 9FeAl_x \quad (1i)$$

For the reactions (1a)–(1i), the molar volumes per mole of oxygen of the reactant oxides range from 9.4 cm$^3$/mol O (for $TiO_2$ as rutile) to 11.7 cm$^3$/mol O (for $Nb_2O_5$), whereas the molar volume of $Al_2O_3$ is 8.5 cm$^3$/mol O [11]. That is, the volume of oxide produced (alumina) by each of these reactions is less than the volume of the oxide that is consumed.

A novel displacement-reaction-based technique for the fabrication of shaped ceramic-metal composites with high ceramic content is demonstrated in this paper: the Displacive Compensation of Porosity (DCP) method [12]. Like the $C^4$, RMP, and AAA methods, a ceramic/metal composite is produced in the DCP process by a displacement reaction between a liquid metal and a solid ceramic. However, unlike these other approaches, the DCP method utilizes displacement reactions that generate more ceramic volume than is consumed. Consider the following general displacement reaction:

$$x\{\mathrm{M}\} + \mathrm{NO}_y(\mathrm{s}) \Rightarrow x\mathrm{MO}_{y/x}(\mathrm{s}) + \{\mathrm{N}\} \qquad (2)$$

where {M} and {N} refer to a fluid metallic reactant and a fluid metallic product, respectively, and $\mathrm{NO}_y$(s) and $\mathrm{MO}_{y/x}$(s) refer to a solid oxide reactant and a solid oxide product, respectively. In the DCP process, the fluid reactant M is allowed to infiltrate a porous preform and react with the oxide phase $\mathrm{NO}_y$ that is present within the preform. Reactions are chosen such that the volume of $x$ moles of the product $\mathrm{MO}_{y/x}$ is larger than the volume of 1 mole of the reactant $\mathrm{NO}_y$. Prior to infiltration, the preform is annealed to allow necks to form between the $\mathrm{NO}_y$ particles, so that the preform becomes rigid. Such neck formation is required to avoid distortion of the preform shape due to particle rearrangement resulting from the capillary pressure generated by a wetting liquid. Upon infiltration, the product $\mathrm{MO}_{y/x}$ can form at internal fluid/solid interfaces. If the increase in ceramic volume associated with $\mathrm{MO}_{y/x}$ formation is accommodated by the prior pore volume of the preform (i.e., reaction-induced densification without sintering), then the external dimensions of the final composite can be close to those of the starting preform (i.e., near net-shape processing). After infiltration, the transformation time should be dependent on the size scale of microstructural features of the preform (e.g., $\mathrm{NO}_y$(s) particle size and surface area, the preform pore size) and not on the external dimensions of the preform. That is, it should be possible to transform relatively large preforms within reasonable reaction times. Cooling from the reaction temperature should then yield a dense, shaped composite of $\mathrm{MO}_{y/x}$(s) and N(s) (or a solid N-M alloy). Although the pores within the starting preform would need to be interconnected to allow for complete pore filling by the infiltrating metallic reactant, the reaction-induced increase in internal ceramic volume could result in a displacement of metallic fluid from the preform, so that the amount of solid metallic phase retained in the final composite could be relatively small. In other words, the DCP reaction could be used to generate composites with higher ceramic contents than could be achieved merely by infiltrating a metallic liquid into a porous preform. Hence, the DCP process could be a simple and attractive means of producing dense, ceramic-rich composites of near net shape.

For this paper, MgO/Mg-Al composites were fabricated by the use of the following DCP-type displacement reaction:

$$3\{\mathrm{Mg}\} + \mathrm{Al_2O_3(s)} = 3\mathrm{MgO(s)} + 2\{\mathrm{Al}\} \qquad (3a)$$

This reaction was chosen as a model system for study because: i) the volume of 3 moles of MgO is 31.8% larger than 1 mole of $Al_2O_3$ [11], ii) prior work has shown that molten magnesium can wet and infiltrate (pressureless) porous $Al_2O_3$ preforms in an inert atmosphere [13], iii) physical data (densities, elastic moduli) are available for solid MgO and Mg-Al alloys [11, 14–16], and iv) thermodynamic data are available for MgO, $Al_2O_3$, and Mg-Al liquids [14, 17]. MgO/Mg-Al composites may also be attractive for applications that require the use of lightweight materials with enhanced stiffness relative to Mg-Al alloys and enhanced toughness relative to MgO. The purpose of this paper is to demonstrate that the DCP process can be used to fabricate dense MgO/Mg-Al composites of high oxide content that retain the shapes and dimensions of starting porous $Al_2O_3$ preforms.

## 2. Experimental

### 2.1. Sample preparation

The DCP processing steps used to produce MgO/Mg-Al composite bodies from sacrificial $Al_2O_3$ preforms are shown in the schematic illustration of Fig. 1.

#### *2.1.1. Alumina preform synthesis*

$Al_2O_3$ powder (99.98% purity, 7 micron ave. size; Johnson-Matthey, Inc., Ward Hill, MA, USA) was mixed with a 4 wt % polyvinyl alcohol (PVA) binder solution, and the mixture was allowed to dry in air at room temperature. The dried mixture, which contained 2 wt % binder, was uniaxially pressed into disks (10 mm diameter × 1.8–2.0 mm thickness) and bars (5 cm × 6 mm × 7 mm) under a peak stress of 1200 MPa. The as-pressed disks and bars were then heated in air at 500 °C for 14.4 ks to remove the PVA binder. Subsequent heat treatment was conducted at $\leq$ 1500 °C for 14.4–28.8 ks in air to convert the preforms into rigid $Al_2O_3$ disks and bars with relative densities of 66–71% and 53–58%, respectively.

#### *2.1.2. Preform infiltration and reaction with molten magnesium*

The porous alumina disks and bars were infiltrated and reacted with molten magnesium. Two semi-circular disks of magnesium (99.95% purity; Johnson-Matthey, Inc.) were placed above and below a given alumina preform. The molar $Mg : Al_2O_3$ ratios of such assemblies were 20–22 : 1 and 6–7 : 1 for the disk-shaped and bar-shaped preforms, respectively. The Mg-$Al_2O_3$ assemblies were placed within 1020 steel tubes (1.4 cm internal diameter × 7.0 cm length; McMaster Carr, Chicago, IL, USA) that were then sealed by welding in air.* The sealed tubes were annealed for 7.2 ks to 54 ks at 1000 °C under a flowing argon atmosphere to allow for magnesium infiltration and reaction with

* Steel was chosen as the canning material because: a) it can sustain a reaction temperature of 1000 °C in flowing argon, b) it could easily be sealed using TIG welding, and c) it has very limited solubility in molten Mg [18].

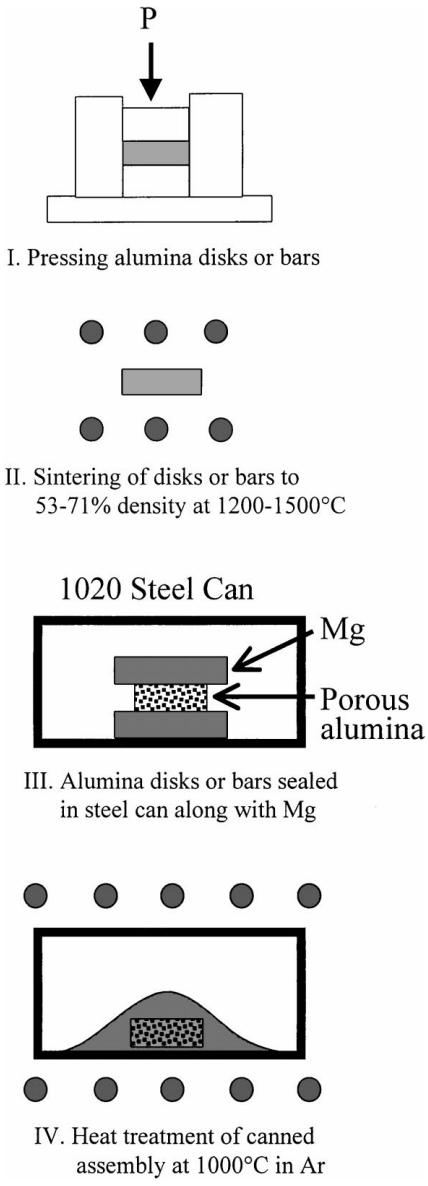


*Figure 1* Schematic illustration of the Displacive Compensation of Porosity (DCP) method for fabricating MgO/Mg-Al composites.

the alumina preforms (note: the specimens were annealed within steel tubes to avoid excessive loss of magnesium by vaporization). After the desired annealing time at 1000 °C, the furnace was turned off and the samples were allowed to cool to room temperature. The steel enclosures were then cut open and the transformed specimens were retrieved. The excess magnesium adhering to the disk- and bar-shaped specimens was removed by applying a shear force (as discussed in reference 13).

## 2.2. Characterization

### *2.2.1. Microstructure and microchemistry*

The microstructures of partially- and completely-transformed specimens were evaluated with optical microscopy, scanning electron microscopy (SEM), and electron microprobe analyses (EPMA). Specimens were cross-sectioned with a diamond saw, mounted in epoxy, and then polished to a 1 micron finish with a series of diamond pastes. Some of the polished samples were etched with a concentrated HCl solution (37.4% HCl) for 360 s to allow for more clear delineation of interphase boundaries. For backscattered and secondary electron imaging, specimens were also sputter coated with gold. Scanning electron microscopy was conducted with a field-emission-gun microscope (Model XL-30, Philips Electronics N. V., Eindhoven, The Netherlands) equipped with a Si/Li detector for qualitative energy-dispersive spectroscopy (Edax International, Mahwah, NJ, USA). Quantitative microchemical analyses were obtained by wavelength-dispersive spectroscopy (WDS) using an electron microprobe (Model SX50, Cameca Instruments, Inc., Trumbull, CT, USA). Pure Mg, Al, and Fe standards (99.99% purity, C.M. Taylor Co., San Jose, CA) were used for WDS analyses. Quantitative evaluations of the phase contents of composite specimens were obtained by two methods: 1) image analyses using ScionImage software (free, public-domain software, available at <http://www.rsb.info.nih.gov/nih-image>, developed by Wayne Rasband at the U.S. National Institutes of Health) and 2) thermal assaying. Thermal assaying was conducted by crushing the transformed, composite specimens into powder with a mortar and pestle and then oxidizing the powder at 550 °C for 43.2 ks, 700 °C for 10.8 ks, and then 700 °C for an additional 10.8 ks, all in pure, flowing oxygen. No weight gain was detected after the second 10.8 ks anneal at 700 °C, which indicated that oxidation of the powder was completed during the first 10.8 ks at this temperature. The weight gain due to oxidation was used to determine the amount of metal that had been present in the composites. The densities of the preforms and composite products were determined using Archimedes method along with bulk (dry weight) measurements. Archimede's measurements were conducted on samples sealed in a paraffin wax film of known density, using doubly-distilled water as the buoyant fluid. X-ray powder diffraction (XRD) analyses (Model PAD V diffractometer, Scintag, Inc., Cupertino, CA, USA) of partially- and completely-transformed specimens were conducted at room temperature with $CuK_\alpha$ radiation using a scanning rate of 1°/min. The MgO diffraction peaks exhibited by the specimens were used as internal XRD standards (i.e., to account for any slight specimen misalignment in the diffractometer). Prior to XRD analyses, specimens were ground into powder with a zirconia mortar and pestle, mixed with X-ray transparent vacuum grease (high vacuum grease, Dow Corning Inc., Midland, MI, USA) and placed on a single crystal silicon substrate. The silicon substrate was ground to expose an irrational plane so as not to generate diffraction peaks within the $2\theta$ range examined (30–65°).

### *2.2.2. Strength, toughness, and hydration resistance*

The flexural strengths of the bar-shaped MgO/Mg-Al composites were obtained by four point bend tests as per ASTM standard C 1161 (configuration A) [19]. MgO/Mg-Al bars were cut and ground to dimensions

of 25 × 2 × 1.5 mm, and the bar surfaces were then polished to a 1 micron finish with a series of diamond pastes. Prior to bending, the four long edges of each bar were uniformly chamfered at 45°. Indentation testing was used to evaluate the fracture toughnesses of the MgO/Mg-Al composites [20]. A load of 147 N was used to push a standard Vickers indentor into specimen surfaces that had been polished to a 1 micron diamond finish. The dimensions of the indent, and the lengths of the cracks emanating from the corners of the indent, were evaluated by secondary electron microscopy. The crack length data obtained from 10 indentations was used to obtain an average value of fracture toughness. The hydration resistance of a given specimen was evaluated by measuring the specimen weight change after exposure to a water-vapor-saturated atmosphere for 86.5 ks at 71 °C (i.e., see ASTM standard C492 [19]).

## 3. Results

### 3.1. Microstructural and microchemical analyses of disk- and bar-shaped specimens

XRD patterns obtained from the bar-shaped samples after infiltration and reaction for 7.2 ks and 36 ks at 1000 °C are shown in Fig. 2a and b, respectively. The pattern in Fig. 2a reveals predominant peaks for MgO, along with smaller peaks for Mg, $Mg_{17}Al_{12}$, and Al (note: the relative intensity of the peak located near $2\theta = 37°$ in Fig. 2a is greater than expected for the (1 1 1) peak of MgO, which is consistent with a superposition of the most intense (1 0 1) peak for Mg). A small amount of $MgAl_2O_4$ may also have been present in the specimen of Fig. 2a (i.e., the most intense (3 1 1) diffraction peak for spinel near $2\theta = 37°$ is overlapped by the (1 1 1) peak for MgO and the (1 0 1) peak for Mg) [11]. The diffraction peaks labeled Mg and $Mg_{17}Al_{12}$ in Fig. 2a and b were shifted to higher and lower values of $2\theta$ (by 0.2–0.3°) respectively, than have been reported for pure Mg and for pure, stoichiometric $Mg_{17}Al_{12}$ [11]. Diffraction peaks for $\alpha$-$Al_2O_3$ (or other alumina polymorphs) or other Mg-Al compounds (e.g., $Al_3Mg_2$, the *R* phase—$Al_{0.58}Mg_{0.42}$, and metastable $Al_2Mg$ [14]) were not detected. Phases similar to those detected in Fig. 2a were observed after 36 ks of reaction (see Fig. 2b).

XRD patterns obtained from disk-shaped specimens after infiltration and reaction for varied times are shown in Fig. 2c–e, respectively. After exposure to molten magnesium for 7.2 ks at 1000 °C, diffraction peaks for Mg, MgO, $Al_2O_3$, and $MgAl_2O_4$ were detected in Fig. 2c [11]. Disk-shaped specimens annealed for 36 ks exhibited predominant diffraction peaks for MgO, with smaller peaks observed for Mg, $MgAl_2O_4$, and $\alpha$-$Al_2O_3$ (Fig. 2d). After 54 ks of exposure, only diffraction peaks for MgO and Mg could be clearly detected (Fig. 2e). The diffraction peaks labeled Mg in Fig. 2e did not exhibit any detectable shift in position relative to the peaks reported for pure Mg [11].

Polished microstructures of a typical porous, bar-shaped $Al_2O_3$ preform (57% dense) after infiltration/reaction for 7.2 ks at 1000 °C are shown in Fig. 3a and b. X-ray maps for magnesium, aluminum, and oxygen corresponding to the backscattered electron image

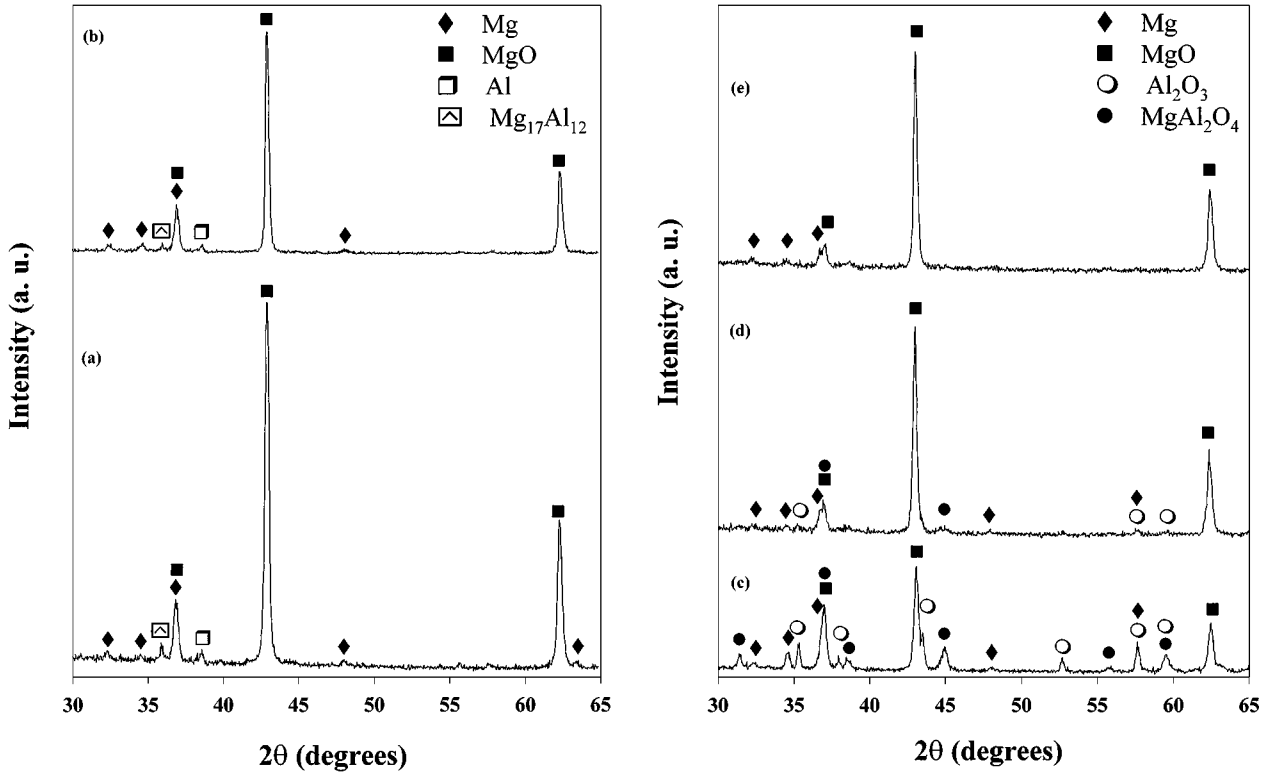


*Figure 2* XRD powder patterns obtained from alumina preforms exposed to molten magnesium at 1000 °C. The patterns in a) and b) were obtained from bar-shaped specimens exposed for 7.2 and 36 ks, respectively. The patterns in c), d), and e) were obtained from disk-shaped specimens exposed for 7.2, 36, and 54 ks, respectively.

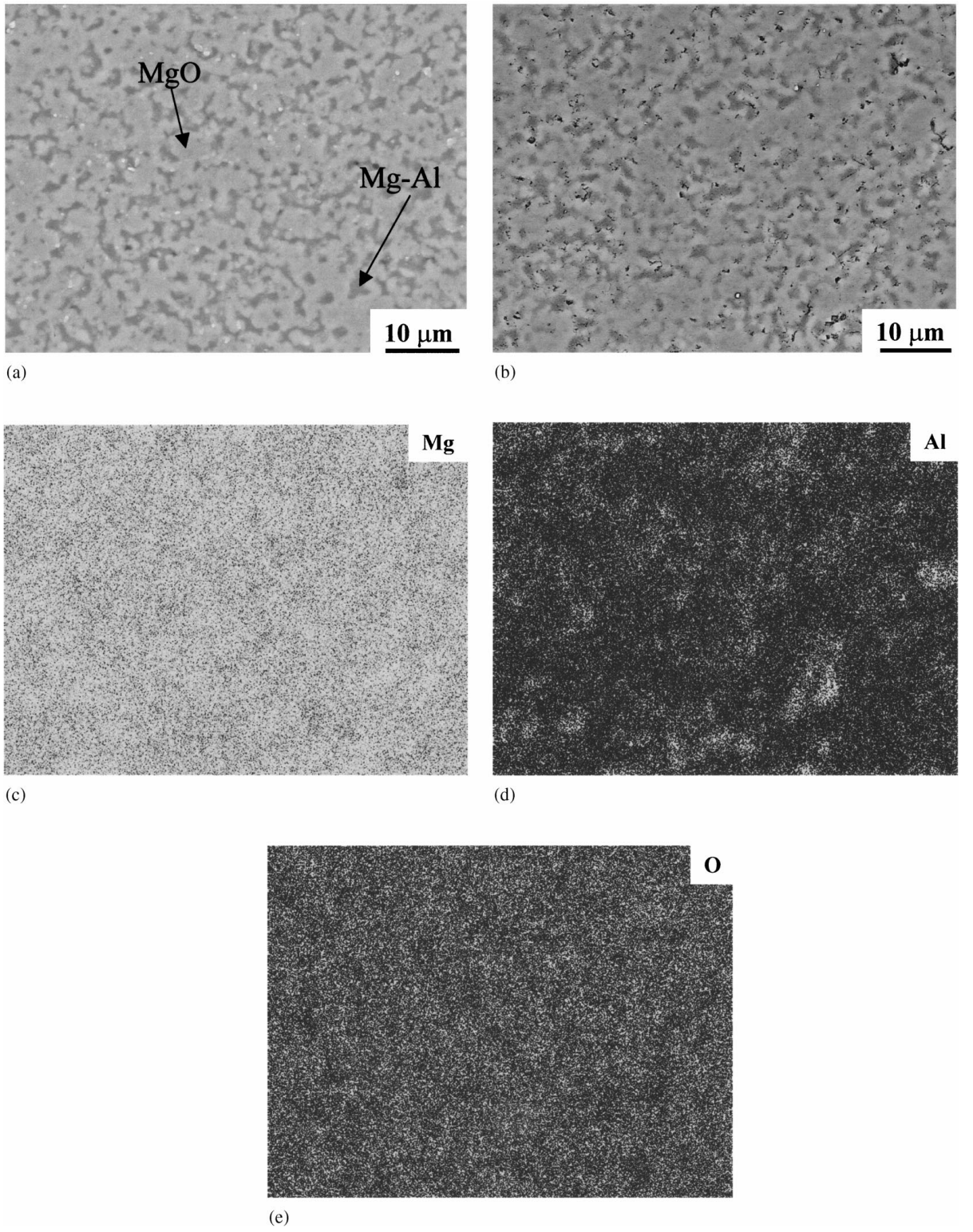


*Figure 3* a) and b) Backscattered electron images of polished cross-sections of bar-shaped preforms after infiltration and reaction with molten magnesium for 7.2 ks at 1000 °C. X-ray maps for magnesium, aluminum, and oxygen associated with the backscattered electron image in b) are shown in c)–e), respectively.

in Fig. 3b are shown in Fig. 3c,d, and e, respectively. The bar-shaped specimen consisted predominantly of MgO (the light phase) with a smaller amount of fine, well-dispersed Mg-Al-bearing metal. Image analyses indicated that the relative amounts of oxide and metal in the specimen of Fig. 3a and b were 73 and 27 vol %, respectively. WDS analyses of the metallic phase in this specimen yielded an average composition of 90.9 at % Mg, 8.6 at % Al, and 0.5 at % Fe. The amount of unreacted $Al_2O_3$ (see Fig. 3d) detected by image analyses of the bar-shaped specimen after 7.2 ks of reaction was 2.0 vol %. Bar-shaped alumina preforms exposed to molten magnesium for 36 ks at 1000 °C exhibited similar microstructures. After exposure to molten

TABLE I Weight, dimensions, and densities of bar- and disk-shaped preforms before and after infiltration/reaction with molten magnesium at 1000 °C (reaction times were ≥7.2 ks for bar-shaped preforms and 54 ks for disk-shaped preforms)

| Sample number | Preform weight (g) | Preform[a] dimensions (mm) | Preform density ($g/cm^3$;% theo.) | Composite weight (g) | Composite[a] dimensions (mm) | Composite Density ($g/cm^3$;% theo.) |
|---|---|---|---|---|---|---|
| 1 (bar) | 4.619 | 50.61 × 6.37 × 6.74 | 2.13; 53.3 | 6.620 | 51.42 × 6.44 × 6.79 | 2.94; 97.7 |
| 2 (bar) | 4.918 | 50.61 × 6.36 × 6.69 | 2.28; 57.2 | 6.829 | 51.23 × 6.40 × 6.84 | 3.04; 98.3 |
| 3 (bar) | 4.382 | 50.58 × 5.86 × 6.36 | 2.32; 58.3 | 6.012 | 51.41 × 5.89 × 6.41 | 3.10; 99.0 |
| 4 (disk) | 0.405 | 9.35 × 2.25 | 2.62; 65.8 | 0.525 | 9.60 × 2.27 | 3.20; 98.6 |
| 5 (disk) | 0.431 | 10.01 × 2.01 | 2.72; 68.4 | 0.547 | 10. 27 × 2.04 | 3.24; 98.3 |
| 6 (disk) | 0.376 | 9.64 × 1.82 | 2.83; 71.0 | 0.466 | 9.89 × 1.84 | 3.30; 98.1 |

[a]Bar dimensions are given as length × width × thickness. Disk dimensions are given as diameter × thickness.

TABLE II Changes in weight, dimensions, volume, and phase content of bar- and disk-shaped preforms after infiltration/reaction with molten magnesium at 1000 °C

| Sample[a] number | Length change (%) | Width change (%) | Thickness change (%) | Diameter change (%) | Volume change (%) | Weight change (%) | Predicted Weight change (%) | MgO content[b] (vol %) | Predicted MgO content (vol %) | Pore volume compensation by MgO (%$P_{oxide}$) |
|---|---|---|---|---|---|---|---|---|---|---|
| 1 (bar) | 1.6 | 1.1 | 0.7 | — | 3.5 | 43.3 | 45.2 | 70.4 | 67.9 | 34.4 |
| 2 (bar) | 1.2 | 2.2 | 0.6 | — | 4.2 | 38.8 | 38.9 | 73.0 | 72.4 | 34.3 |
| 3 (bar) | 1.6 | 0.8 | 0.5 | — | 3.0 | 37.2 | 38.1 | 73.8 | 74.6 | 35.3 |
| 4 (disk) | — | — | 0.9 | 2.7 | 6.4 | 29.6 | 30.6 | 79.9 | 81.5 | 37.5 |
| 5 (disk) | — | — | 1.5 | 2.6 | 6.8 | 26.9 | 28.0 | 83.4 | 84.4 | 43.9 |
| 6 (disk) | — | — | 1.1 | 2.6 | 6.4 | 23.9 | 25.2 | 85.6 | 88.0 | 47.2 |

[a]Same samples as in Table I. [b]As determined from image analyses.

Mg for 7.2-36 ks at 1000 °C, the resulting bar-shaped MgO/Mg-Al composites possessed bulk densities of 2.94–3.10 $g/cm^3$, which corresponded to relative densities of 97.7–99.0% (see Table I).

The microstructure of a typical porous, disk-shaped $Al_2O_3$ preform (71% dense) before infiltration is shown in Fig. 4a. Backscattered electron images of the microstructure produced after infiltration/reaction of molten Mg with such disk-shaped preforms at 1000 °C for 36 ks are shown in Fig. 4b and c. The polished cross-sections shown in Fig. 4b and c were etched to remove the metallic phase and to reveal oxide-oxide boundaries. X-ray maps for magnesium, aluminum, and oxygen corresponding to the backscattered electron image in Fig. 4c are shown in Fig. 4d,e, and f, respectively. The microstructure produced after 54 ks of reaction is shown in Fig. 4g. X-ray maps associated with the backscattered electron image in Fig. 4g are presented in Fig. 4h–j. The specimens shown in Fig. 4b,c, and g consisted predominantly of MgO. The X-ray maps in Fig. 4d–f and 4h–j also revealed oxide particles that were enriched in aluminum and depleted in magnesium. EDS analyses revealed that these particles consisted of $Al_2O_3$. Image analyses indicated that the amounts of unreacted alumina in the specimens of Fig. 4c and g were 8.1 and 3.3 vol %, respectively. Such unreacted alumina particles could also be observed in the higher-magnification etched cross-section shown in Fig. 4b. WDS analyses of the metallic phase in the specimen of Fig. 4g yielded a composition of 99.2 at % Mg, 0.5 at % Al, and 0.3 at % Fe. Image analyses indicated that the relative amounts of oxide and metal in the specimen of Fig. 4g were 85.6 vol % and 14.4 vol %, respectively. After exposure to molten Mg for 54 ks at 1000 °C, the resulting disk-shaped MgO/Mg-Al composites possessed bulk densities of 3.20–3.30 $g/cm^3$, which corresponded to relative densities of 98.1–98.6% (see Table I).

Microchemical analyses were also conducted on the internal surfaces of the steel can after reaction at 1000 °C. At certain locations, the composition of the can surface was found to contain appreciable aluminum (i.e., up to about 20 at % Al). An EDX spectrum obtain from such a surface analysis is shown in Fig. 5.

## 3.2. Weight, dimensional, and density changes upon transformation of disk- and bar-shaped specimens

The weights, dimensions, and densities of several disk- and bar-shaped preforms, and of corresponding transformed specimens, are presented in Table I. The changes in weight, dimensions, and volume upon transformation, and the measured magnesia contents of these specimens are listed in Table II. Predicted values of weight change and magnesia content (see discussion section) are also listed in Table II. The measured magnesia contents (from image analyses) and weight changes of the transformed specimens were in good agreement with the predicted values. Independent confirmation of the magnesia contents obtained by image analyses was obtained on a few samples by thermal assaying. Weight change measurements upon complete oxidation indicated that the bar-shaped specimens 1 and 2 in Table II

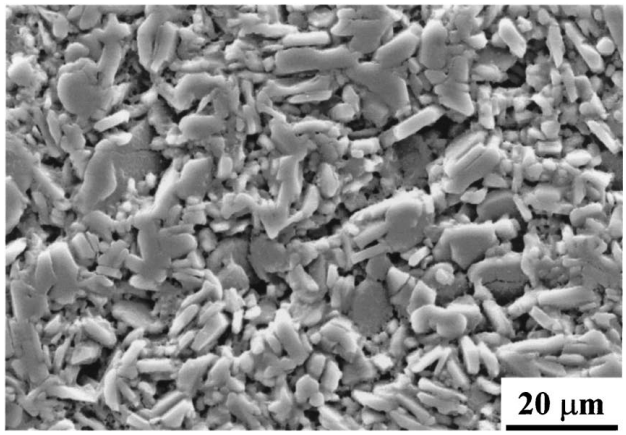


(a)

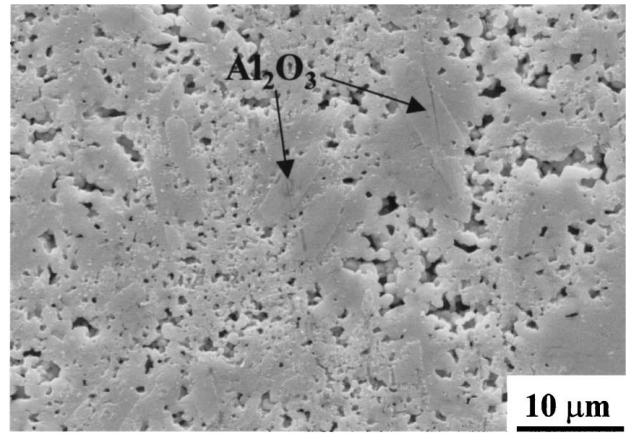


(b)

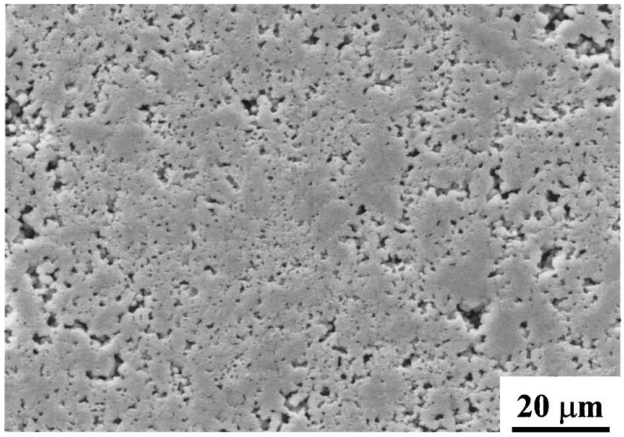


(c)

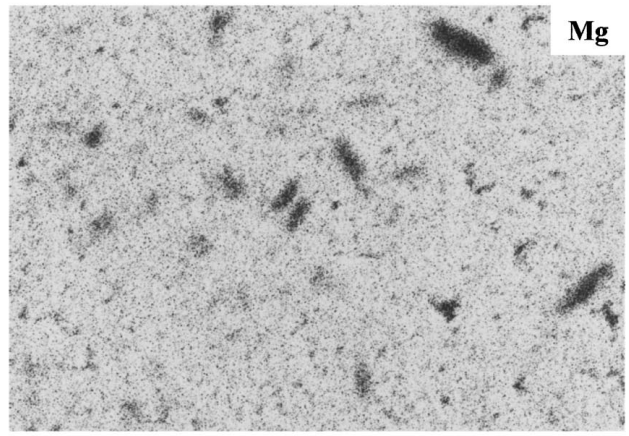


(d)


(e)

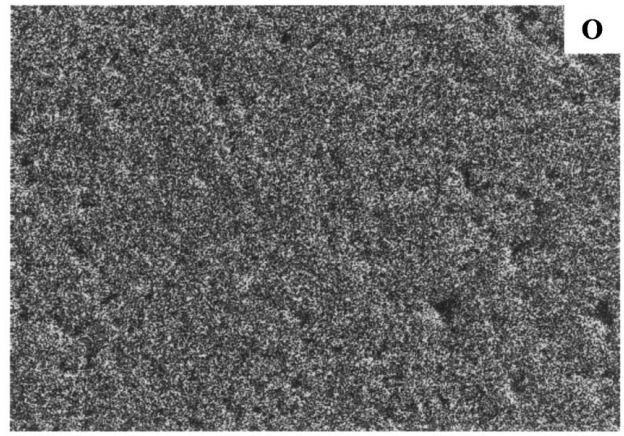


(f)

*Figure 4* a) Secondary electron image of a polished cross-section of a rigid, 71% dense, disk-shaped alumina preform. b) and c) Backscattered electron images of polished and chemically-etched cross-sections of disk-shaped preforms after infiltration and reaction with molten magnesium for 36 ks at 1000 °C. X-ray maps for magnesium, aluminum, and oxygen associated with the backscattered electron image in c) are shown in d)–f), respectively. g) Backscattered electron image of a polished cross-section of a disk-shaped preform after infiltration and reaction with molten magnesium for 54 ks at 1000 °C. X-ray maps for magnesium, aluminum, and oxygen associated with the backscattered electron image in g) are shown in h)–j), respectively. (*Continued*)

consisted of 67.1 and 74.1 vol % MgO, respectively, which were similar to the values obtained by image analyses.

Optical photographs of disk- and bar-shaped preforms before and after conversion into composite specimens are shown in Fig. 6a–d. The transformed specimens retained the shapes and dimensions (to within 2.7%, see Table II) of the starting preforms. The edges of the transformed composites were sharp and no macrocracks were observed.

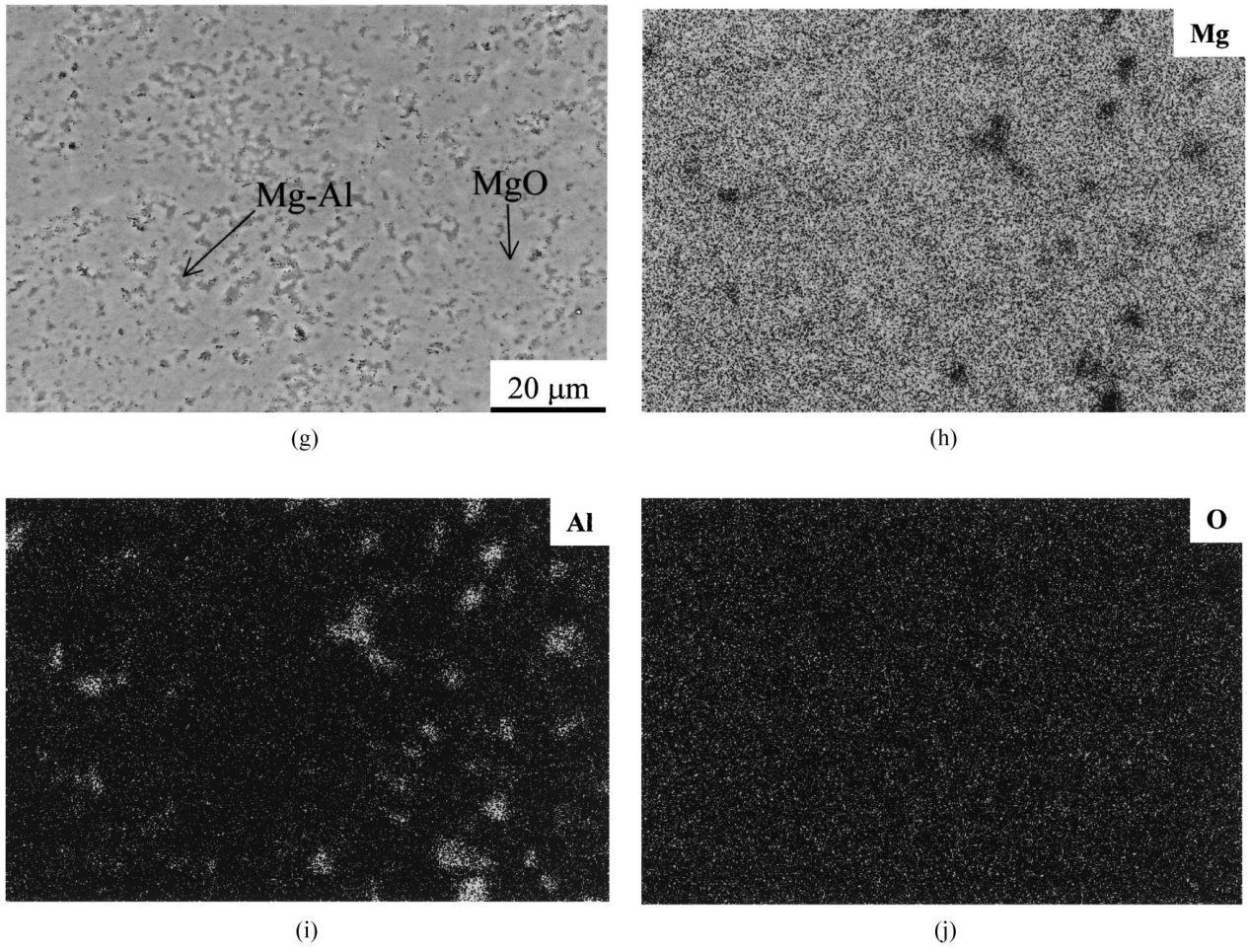


*Figure 4* (*Continued*).

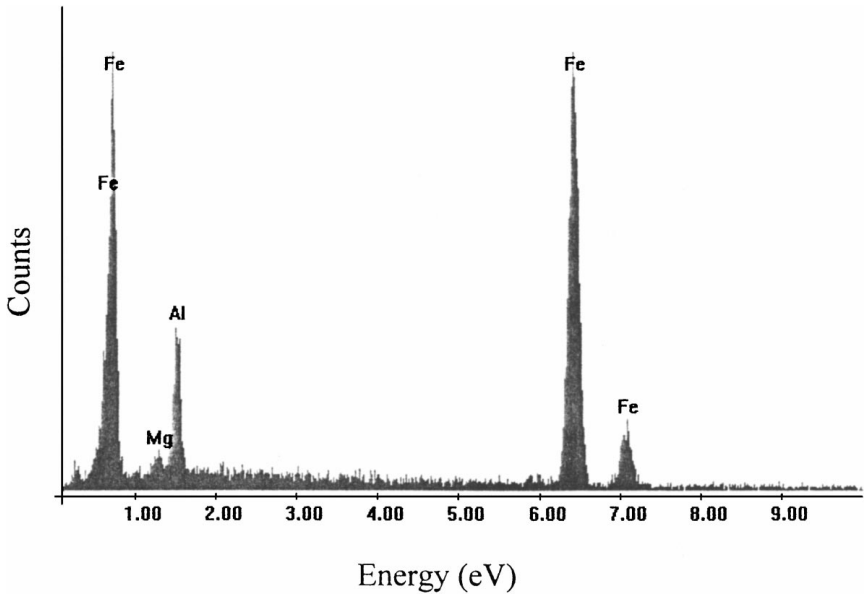


*Figure 5* EDX spectrum obtained from the internal surface of a steel can exposed to liquid magnesium for 54 ks at 1000 °C.

### 3.3. Mechanical properties and hydration resistance

The flexural strengths, indentation toughnesses, and hydration resistances of composite specimens similar to sample number 3 in Tables I and II (i.e., relative densities of 99 ± 1%, magnesia contents of 73.8 ± 3.8 vol %) were evaluated. Four point bend test measurements of 7 bar-shaped composites yielded an average strength of 244.3 MPa, with a range of 186–319 MPa. Indentation measurements [20] yielded an average fracture

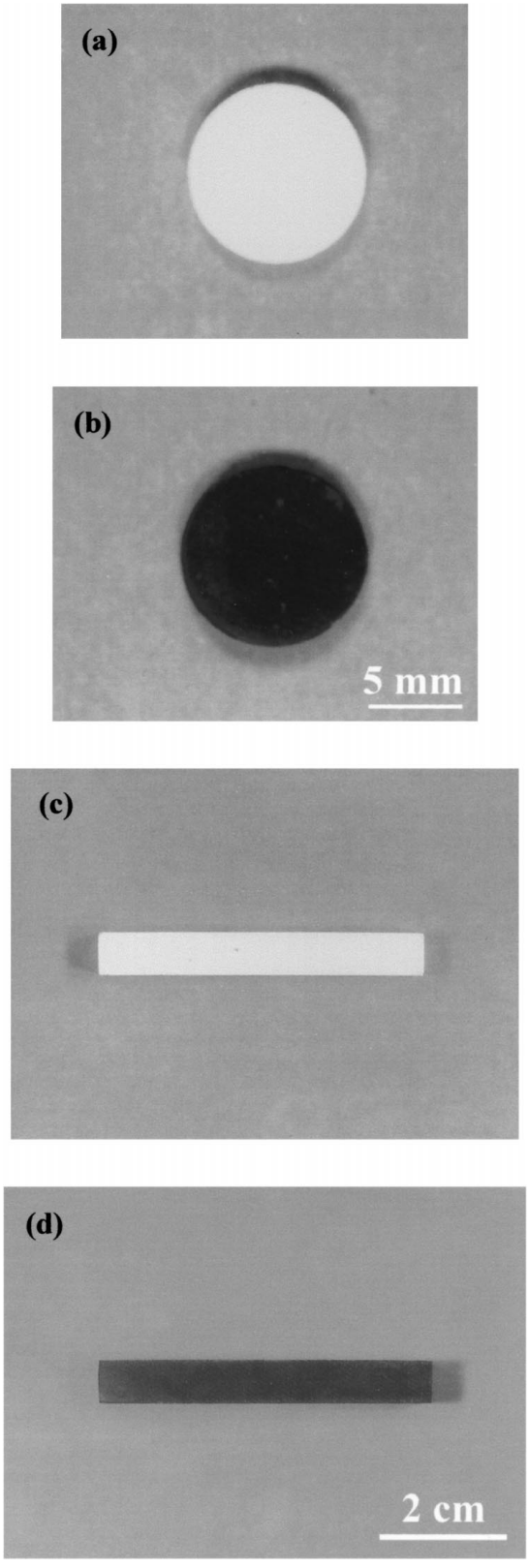


*Figure 6* Optical photographs of a rigid, disk-shaped alumina preform: a) before infiltration and b) after infiltration and reaction with molten magnesium for 54 ks at 1000 °C. Optical photographs of a rigid, bar-shaped alumina preform: c) before infiltration, and d) after infiltration and reaction with molten magnesium for 7.2 ks at 1000 °C.

toughness value of 5.4 MPa · $m^{1/2}$ (range = 4.6–7.2 MPa · $m^{1/2}$). Four composite specimens were exposed for 86.4 ks to a water-vapor-saturated atmosphere at 71 °C [19]. No weight change could be detected for three of these specimens, and a fourth specimen exhibited a weight gain of only 0.04%.

## 4. Discussion

### 4.1. Thermodynamics of the net displacement reaction

Molten magnesium can react with alumina to yield magnesia as per the following net reaction:

$$3\{Mg\} + Al_2O_3(s) = 3MgO(s) + 2\{Al\} \quad (3a)$$

where the brackets refer to species present in a liquid solution. If the solid phases are assumed to be present in their reference states (i.e., if pure, solid oxide reference states are chosen for magnesia and alumina), then the standard Gibbs free energy change for this reaction, $\Delta G^0_{rxn(3a)}$, at 1000 °C is given by [17]:

$$\Delta G^0_{rxn(3a)} = -10{,}584\{2\ln[\gamma_{Al}(1 - X_{Mg})] - 3\ln[\gamma_{Mg}X_{Mg}]\} = -112{,}723\ J/mol \quad (1a)$$

The excess molar Gibbs free energy of mixing, $G^E_m$, of liquid Mg-Al solutions at 1000 °C can be expressed as [14]:

$$G^E_m(1000\,^\circ C) = -1{,}408X_{Mg} + 1034(X_{Mg})^2 + 374(X_{Mg})^3\ J/mol \quad (2)$$

Hence, the partial excess molar Gibbs free energy of mixing of Mg, $G^E_{Mg}$, and of Al, $G^E_{Al}$, can be expressed at 1000 °C as:

$$G^E_{Mg}(1000\,^\circ C) = -1{,}408 + 2067X_{Mg} + 89(X_{Mg})^2 - 748(X_{Mg})^3\ J/mol = 10{,}584\ln[\gamma_{Mg}] \quad (3a)$$

$$G^E_{Al}(1000\,^\circ C) = -1033(X_{Mg})^2 - 748(X_{Mg})^3\ J/mol = 10{,}584\ln[\gamma_{Al}] \quad (3b)$$

Simultaneous solution of Equations 1, 3a, and 3b indicates that reaction (3a) should proceed spontaneously to the right at 1000 °C, if the magnesium concentration in the Mg-Al solution exceeds 3.2 at %. In the present work, the magnesium concentration of the liquid was maintained at ≥90.9 at %, so that net reaction (3a) was thermodynamically favored at 1000 °C.

### 4.2. Spinel formation, alumina consumption, and metallic phase formation

After exposure to liquid magnesium for 7.2 ks at 1000 °C, the disk-shaped samples exhibited diffraction peaks for two magnesia-bearing phases: MgO and $MgAl_2O_4$ (see Fig. 2c). The intensities of the spinel diffraction peaks decreased as the reaction time increased to 36 ks (Fig. 2d) and, after 54 ks, the peaks for spinel could not be detected (Fig. 2e). The formation and then loss of spinel with increasing reaction time indicated that spinel was produced as an intermediate reaction product. Consider the following reactions at

1000 °C (note: net reaction (3a) is obtained from the sum of reactions (3b) and (3c)):

$$3/4\{Mg\} + Al_2O_3(s) = 3/4MgAl_2O_4(s) + 1/2\{Al\} \quad (3b)$$

$$9/4\{Mg\} + 3/4MgAl_2O_4(s) = 3MgO(s) + 3/2\{Al\} \quad (3c)$$

The standard Gibbs free energy changes for these reactions at 1000 °C are given by (again assuming that the solid phases are present in their pure, solid oxide reference states) [17]:

$$\Delta G^0_{rxn(3b)} = -10{,}584\{1/2\ln[\gamma_{Al}(1 - X_{Mg})] - 3/4\ln[\gamma_{Mg}X_{Mg}]\} = -48{,}082\ J/mol \quad (1b)$$

$$\Delta G^0_{rxn(3c)} = -10{,}584\{3/2\ln[\gamma_{Al}(1 - X_{Mg})] - 9/4\ln[\gamma_{Mg}X_{Mg}]\} = -64{,}641\ J/mol \quad (1c)$$

Simultaneous solution of Equations 3a, 3b, and 1b or 1c indicates that reactions (3b) and (3c) should proceed spontaneously to the right at 1000 °C, if the magnesium concentration in the Mg-Al solution exceeds 0.27 at % and 7.1 at %, respectively. That is, less magnesium is required in the melt at 1000 °C in order for reaction (3b) to proceed spontaneously to the right than for the net reaction (3a). Hence, it was possible for spinel to form as an intermediate reaction product at alumina/melt interfaces in the present work. However, since the magnesium concentration in the melt exceeded 7.1 at %, reaction (3c) was also thermodynamically favored, so that any spinel that would have initially formed should have been gradually consumed to produce magnesia. The formation of spinel as an intermediate reaction product during the reaction of molten magnesium with alumina at 1000 °C has also been reported by Jynge and Motzfeldt [21].

The XRD and microstructural analyses indicated that the alumina within the disk-shaped specimens was nearly completely consumed after 54 ks of reaction with molten magnesium at 1000 °C; that is, the amount of unreacted alumina in the disk-shaped specimens decreased from 8.1 to 3.3 vol % as the reaction time was increased from 36 to 54 ks. For the bar-shaped specimens, however, only 7.2 ks was required to consume 98% of the alumina at 1000 °C. The relatively short time required for alumina consumption in the bar-shaped specimens is likely to have been due to the higher porosity (i.e., more internal liquid metal reactant after infiltration) and the reduced amount of alumina in these specimens relative to the disk-shaped samples.

The disk-shaped composite specimens exhibited diffraction peaks for only MgO and Mg after 54 ks of reaction with molten magnesium at 1000 °C (Fig. 2e). Microprobe analyses indicated that the magnesium-bearing phase in these composites contained small amounts of aluminum and iron (e.g., 0.5 at % Al and 0.3 at % Fe). In other words, some of the aluminum liberated by the net reaction (3a) dissolved into the molten magnesium and was retained in the solid-solution magnesium alloy upon solidification. However, the aluminum content of the magnesium alloy in these composites was less than expected from reaction (3a). The molar Mg:$Al_2O_3$ ratio used for the reaction couples involving the disk-shaped alumina preforms was 20–22 : 1. Hence, if all of the alumina in the disk-shaped preforms was consumed as per reaction (3a), then equilibration of the liberated aluminum with the remaining magnesium should have yielded an alloy consisting of 89.5–90.5 at % Mg and 10.5–9.5 at % Al. The presence of only 0.5 at % Al in the magnesium alloy of the disk-shaped composites was attributed to the reaction of aluminum in the liquid at 1000 °C with the steel can. Chemical analyses of the internal surface of the steel can (Fig. 5) revealed that an appreciable amount of aluminum had dissolved into the can. This is not surprising, given the relatively high solid solubility of aluminum in iron at 1000 °C (≈28 at % Al in $\alpha$-Fe and ≈28 to 53.5 at % in FeAl [18]).† The presence of some iron in the magnesium alloy indicated that a small amount of iron had dissolved into the liquid metal at 1000 °C. The solubility of iron in molten magnesium at 1000 °C is reported to be about 0.13 at % at 1000 °C [18], which is not far from the measured iron content of the magnesium alloy (note: the solubility of iron in Mg-rich, Mg-Al melts has not been reported).

Diffraction peaks for MgO, Mg, and $Mg_{17}Al_{12}$ were detected in the bar-shaped composites after 7.2 and 36 ks of reaction at 1000 °C. The diffraction peaks labeled Mg and $Mg_{17}Al_{12}$ in Fig. 2a and b were shifted to higher and lower values of $2\theta$, respectively, than expected for pure Mg and for pure, stoichiometric $Mg_{17}Al_{12}$ [11], which was consistent with the presence of an Mg-Al solid solution and Mg-excess $Mg_{17}Al_{12}$. The metallic phase in the bar-shaped composites was enriched in magnesium, with lesser amounts of aluminum and iron (e.g., 8.6 at % Al and 0.5 at % Fe). As was the case for the disk-shaped composites, the actual aluminum content of the metal was less than expected from reaction (3a), owing to the reaction of the steel can with the aluminum in the melt. The magnesium content of the metal in the bar-shaped composites after 7.2 ks of reaction was less than for the disk-shaped composites after 54 ks of reaction. This composition difference was attributed to the reduced time for reaction of the aluminum in the molten metal with the steel can and to the lesser amount of Mg placed in contact with the bar-shaped preforms (i.e., a molar Mg:$Al_2O_3$ ratio of 6–7 : 1 was used for the bar-shaped alumina preforms, as opposed to 20–22 : 1 for the disk-shaped preforms). The presence of $Mg_{17}Al_{12}$ in the bar-shaped specimens was consistent with the measured composition of the metal remaining within these specimens. That is, cooling of a metallic liquid with a composition of 90.5 at % Mg and 8.6 at % Al to temperatures below about 390 °C should have resulted in the crystallization of a mixture of Mg-excess $Mg_{17}Al_{12}$ and an Al-rich Mg-Al solid solution (as was detected in Fig. 2a and b) [14].

† Because the aluminum content of the can varied considerably with position on the internal surface of the can, no effort was made to determine the total amount of aluminum dissolved into the steel can.

## 4.3. Mass and volume conservation

In order to predict the phase contents of the MgO/Mg-Al composites that should be produced upon infiltration and reaction of porous alumina preforms with molten magnesium, equations describing the conservation of mass and volume need to be developed.

### *4.3.1. Theoretical density and composite phase content*

Consider a porous $Al_2O_3$ preform with a relative density (% of theoretical) of $\rho_{rel}$ and a total volume (solid + pores) of 100 $cm^3$. The number of moles, $n_{Al_2O_3}$, the weight, $W_{Al_2O_3}$, and the volume, $V_{Al_2O_3}$, of solid $Al_2O_3$ in such a preform are given by:

$$n_{Al_2O_3} = \rho_{rel}/V_{m,Al_2O_3} \quad (4a)$$

$$W_{Al_2O_3} = M_{Al_2O_3}\rho_{rel}/V_{m,Al_2O_3} \quad (4b)$$

$$V_{Al_2O_3} = \rho_{rel} \quad (4c)$$

where $V_{m,Al_2O_3}$ and $M_{Al_2O_3}$ refer to the molar volume (25.58 $cm^3$/mol [11]) and the molecular weight (101.96 g/mol) of alumina, respectively. According to the net reaction (3a), 3 moles of MgO are produced for every mole of $Al_2O_3$ consumed. Hence, the number of moles, $n_{MgO}$, the mass, $W_{MgO}$, and the volume, $V_{MgO}$, of solid MgO produced upon completion of reaction (3a) are given by:

$$n_{MgO} = 3\rho_{rel}/V_{m,Al_2O_3} \quad (5a)$$

$$W_{MgO} = 3M_{MgO}\rho_{rel}/V_{m,Al_2O_3} \quad (5b)$$

$$V_{MgO} = 3\rho_{rel}(V_{m,MgO}/V_{m,Al_2O_3}) \quad (5c)$$

where $V_{m,MgO}$ and $M_{MgO}$ refer to the molar volume (11.24 $cm^3$/mol [11]) and the molecular weight (40.31 g/mol) of magnesia, respectively. If $\Delta V$ is the increase in the preform volume upon transformation (as determined by measuring the change in the specimen dimensions), then the total volume (solid + pores) of the transformed composite body, $V_{comp}$, will be (100 + $\Delta V$). Because a completely-transformed composite body should be comprised of a mixture of MgO and Mg-bearing metallic phases, the volume of the Mg-bearing metallic phases, $V_{metal}$, in a theoretically-dense composite should be equal to the total composite volume, $V_{comp}$, less the volume of the MgO in the composite, $V_{MgO}$. That is,

$$V_{Metal} = V_{comp} - V_{MgO} = (100 + \Delta V) - 3\rho_{rel}(V_{m,MgO}/V_{m,Al_2O_3}) \quad (6a)$$

The mass of this volume of metal, $W_{Metal}$, in such a theoretically-dense composite, is given by:

$$W_{Metal} = (M_{Metal}/V_{m,Metal}) \times [(100 + \Delta V) - 3\rho_{rel}(V_{m,MgO}/V_{m,Al_2O_3})] \quad (6b)$$

where $M_{Metal}$ and $V_{m,Metal}$ refer to the molecular weight and molar volume, respectively, of the metallic phase. The molecular weights and molar volumes of the metallic phases detected in the bar and disk-shaped specimens were evaluated with the use of the measured compositions and lattice parameter data [11, 14]. The theoretical density, $\rho_{theo}$, of a composite of MgO and Mg-bearing metal produced from a porous alumina preform can be calculated as:

$$\rho_{theo} = \{W_{Metal} + W_{MgO}\}/\{V_{Metal} + V_{MgO}\} \quad (7)$$

or, by combining Equations 5b, 5c, 6a, 6b, and 7, one obtains:

$$\rho_{theo} = (M_{Metal}/V_{m,Metal}) + 3(\rho_{rel}/V_{m,Al_2O_3}) \times [M_{MgO} - (M_{metal}V_{m,MgO}/V_{m,Metal})] \times [1/(100 + \Delta V)] \quad (8)$$

The volume fractions of MgO, $F_{MgO}$, in the composites produced by reaction (3a) are then obtained with the following equation:

$$F_{MgO} = 3\rho_{rel}(V_{m,MgO}/V_{m,Al_2O_3})/(100 + \Delta V) \quad (9)$$

The predicted values of $F_{MgO}$ calculated from Equation 9 are shown in Table II. The predicted $F_{MgO}$ values were within a few percent of the experimentally-measured magnesia volume fractions (by image analyses) of the composite specimens. This agreement was considered good, given the experimental error associated with image analyses (on the order of a few volume percent) and the small amount of residual alumina (a few volume percent or less) retained in the bar- and disk-shaped specimens. As expected from Equation 9, the volume fraction of magnesia in the composites increased as the relative density of the starting alumina preform increased (i.e., as the alumina available for reaction per unit volume of preform increased, more magnesia could be generated per unit volume within the composite).

### *4.3.2. Mass gain upon transformation*

Two factors were responsible for the increase in the mass of the $Al_2O_3$ preforms upon transformation into MgO/Mg-Al composites: a) the conversion of $Al_2O_3$ into MgO (i.e., the mass of 3 moles of MgO is 18.6% greater than the mass of 1 mole of $Al_2O_3$) and b) the filling of pores with Mg-Al metal. The mass of MgO produced from the $Al_2O_3$ present in 100 $cm^3$ of a $\rho_{rel}$% dense preform can be calculated from Equation 5b above. The mass of Mg-Al metal present in a transformed composite that possesses $P$% porosity

can be obtained by the following modification of Equation 6b:

$$W_{\text{Metal}} = [1 - (P/100)](M_{\text{Metal}}/V_{\text{m,Metal}}) \times [(100 + \Delta V) - 3\rho_{\text{rel}}(V_{\text{m,MgO}}/V_{\text{m,Al}_2\text{O}_3})] \quad (10)$$

Hence, the total mass of a (100-$P$)% dense MgO/Mg-Al composite, $W_{\text{Comp}}$, can be expressed as:

$$\begin{aligned} W_{\text{Comp}} &= W_{\text{MgO}} + W_{\text{Metal}} \\ &= 3(M_{\text{MgO}}\rho_{\text{rel}}/V_{\text{m,Al}_2\text{O}_3}) + [1 - (P/100)] \\ &\quad \times (M_{\text{Metal}}/V_{\text{m,Metal}})[(100 + \Delta V) \\ &\quad - 3\rho_{\text{rel}}(V_{\text{m,MgO}}/V_{\text{m,Al}_2\text{O}_3})] \end{aligned} \quad (11)$$

The initial mass of the $Al_2O_3$ preform, $W_{\text{Al}_2\text{O}_3}$, is given by Equation 4b. The mass change, $\Delta W$%, can therefore be calculated from the following equation:

$$\Delta W\% = 100 \cdot (W_{\text{Comp}} - W_{\text{Al}_2\text{O}_3})/W_{\text{Al}_2\text{O}_3} \quad (12a)$$

The predicted weight changes calculated from Equations 4b, 11, and 12a are listed in Table II. The measured weight changes were within a few percent of the predicted values.

Comparison of the data in Tables I and II indicates that the weight gain upon transformation decreased as the relative density of the alumina preforms ($\rho_{\text{rel}}$) increased. The percentage mass gain associated with the formation of magnesia from alumina, $\Delta W_{\text{oxide}}$%, is independent of the starting preform density. This can be seen from the following equation:

$$\begin{aligned} &\Delta W_{\text{oxide}}\% \\ &= [W_{\text{MgO}} - W_{\text{Al}_2\text{O}_3}]/W_{\text{Al}_2\text{O}_3} \\ &= 100 \cdot [3(M_{\text{MgO}}\rho_{\text{rel}}/V_{\text{m,Al}_2\text{O}_3}) \\ &\quad - (M_{\text{Al}_2\text{O}_3}\rho_{\text{rel}}/V_{\text{m,Al}_2\text{O}_3})]/(M_{\text{Al}_2\text{O}_3}\rho_{\text{rel}}/V_{\text{m,Al}_2\text{O}_3}) \\ &= 100 \cdot [3M_{\text{MgO}} - M_{\text{Al}_2\text{O}_3}]/M_{\text{Al}_2\text{O}_3} = 18.6\% \end{aligned} \quad (12b)$$

On the other hand, the percentage mass gain associated with the incorporation of Mg-Al metal into the preform, $\Delta W_{\text{metal}}$%, should decrease with increasing preform density, as indicated by the following equation:

$$\begin{aligned} &\Delta W_{\text{metal}}\% \\ &= (W_{\text{Metal}} - W_{\text{Al}_2\text{O}_3})/W_{\text{Al}_2\text{O}_3} \\ &= 100 \cdot \{[1 - (P/100)](M_{\text{Metal}}/V_{\text{m,Metal}}) \\ &\quad \times [(100 + \Delta V) - 3\rho_{\text{rel}}(V_{\text{m,MgO}}/V_{\text{m,Al}_2\text{O}_3})] \\ &\quad - (M_{\text{Al}_2\text{O}_3}\rho_{\text{rel}}/V_{\text{m,Al}_2\text{O}_3})\}/(M_{\text{Al}_2\text{O}_3}\rho_{\text{rel}}/V_{\text{m,Al}_2\text{O}_3}) \\ &= \{[100 - P][M_{\text{Metal}}/(M_{\text{Al}_2\text{O}_3}V_{\text{m,Metal}})] \\ &\quad \times [(100 + \Delta V)(V_{\text{m,Al}_2\text{O}_3}/\rho_{\text{rel}}) - 3V_{\text{m,MgO}}]\} - 1 \end{aligned} \quad (12c)$$

In other words, a decrease in the pore volume of the preform results in a decrease in the volume available for metal occupancy, so that the weight gain upon conversion decreases with increasing preform density.

#### 4.3.3. Pore volume compensation by MgO formation

As indicated in Table I, the final MgO/Mg-Al composites were 97.7–99.0% dense. These high values of relative density were achieved by filling the pores present in the starting alumina preforms with MgO and Mg-Al metal. The following equation was used to determine the percentage of the pore volume that was compensated by the increase in oxide volume associated with the net reaction (3a):

$$\begin{aligned} \%P_{\text{oxide}} &= 100 \cdot [V_{\text{pore,preform}} - (V_{\text{Comp}} \\ &\quad - V_{\text{MgO}})]/V_{\text{pore,preform}} \\ &= 1 + [(V_{\text{MgO}} - V_{\text{Comp}})/V_{\text{pore,preform}}] \end{aligned} \quad (13)$$

where $V_{\text{pore,preform}}$ refers to the pore volume within a given preform, and the term ($V_{\text{Comp}} - V_{\text{MgO}}$) refers to the non-oxide volume of the composite (i.e., the pore volume of the preform that was not compensated by the increase in oxide volume from reaction (3a)). Experimental values of $\%P_{\text{oxide}}$ were obtained by inserting data from Tables I and II (i.e., the relative preform densities, the total preform volumes, the volume fraction of magnesia in the composites, and the total composite volumes) into Equation 13. As indicated by the $\%P_{\text{oxide}}$ values shown in Table II, about 1/3 to 1/2 of the pore volume in the preforms was effectively filled by the increase in oxide volume associated with reaction (3a). Because the reaction-induced increase in oxide volume was accommodated by the prior pore volume within the preforms, little change occurred in the external specimen dimensions upon transformation. The value of $\%P_{\text{oxide}}$ was found to increase as the relative density of the preform, $\rho_{\text{rel}}$, increased. This trend was expected, as the volume of porosity in the preform, $V_{\text{pore,preform}}$, and the volume of magnesia produced in the composite, $V_{\text{MgO}}$, should decrease and increase, respectively, with an increase in $\rho_{\text{rel}}$ (see Equation 13).

### 4.4. Composite properties

As demonstrated in the present work, the DCP method can yield dense (≥97.7% of theoretical), lightweight ($\rho = 2.94$–$3.30$ g/cm$^3$), oxide-rich (70.4–85.6 vol % MgO) composites at a relatively modest processing temperature (1000 °C) ). MgO/Mg-Al composites containing 70.4 to 79.9 vol % oxide consisted of interpenetrating, co-continuous networks of both oxide and metal (the continuity of the metallic phase in these specimens was confirmed with electrical conductivity measurements). The Mg-Al alloys within composites comprised of 83.4 and 85.6 vol % MgO were discontinuous (i.e., these composites were found to be electrically insulating). Ceramic/metal composites with discontinuous metal phases cannot be produced by other

displacement reaction-based processes (e.g., the C$^4$ [1, 2], AAA [3–5], or RMP [6–10] processes) or by melt infiltration processing.

The values of flexural strength (186–319 MPa, ave. = 244 MPa) and fracture toughness (4.6–7.2 MPa $\cdot$ m$^{1/2}$, ave. = 5.4 MPa $\cdot$ m$^{1/2}$) obtained from the DCP-derived, bar-shaped MgO/Mg-Al (73.8 $\pm$ 3.8 vol % MgO) composites were comparable to the range of values obtained by other authors for $Al_2O_3$/Al composites of similar oxide content [7, 22]. For example, Ewsuk, *et al.* [7] reported flexural strengths (4 point bending) of 280–410 MPa and toughnesses of 5–9 MPa $\cdot$ m$^{1/2}$ for $Al_2O_3$/Al(Si) composites comprised of 70–85 vol % oxide. Tai, *et al.* [22] reported average flexural strengths (3-point bending) of 145–212 MPa and toughnesses of 2.6–3.4 MPa $\cdot$ m$^{1/2}$ for $Al_2O_3$/Al composites comprised of 85 vol % $Al_2O_3$.

The DCP-derived MgO/Mg-Al composites possessed densities in excess of 97.7% of theoretical. Such high relative densities endowed the composites with excellent resistance to hydration. That is, the low exposed surface area of magnesia in such composites resulted in relatively slow hydration rates (i.e., weight gains of 0–0.04% after exposure to water vapor for 86.5 ks at 71 °C). The hydration rate could be further reduced by altering the DCP process so as to produce $MgAl_2O_4$/Mg-Al (MgO-free) composites. The thermodynamic calculations presented in Section 4.1 above indicated that the formation of MgO at 1000 °C can be avoided by keeping the Mg content of the melt below 7.1 at %. That is, $MgAl_2O_4$/Mg-Al composites could be fabricated by reacting $Al_2O_3$ preforms with Mg-Al melts containing between 0.27 and 7.1 at % magnesium. By adjusting the melt composition and preform phase content, the DCP method has recently been used to produce co-continuous $MgAl_2O_4$/Fe-Ni-Al-bearing composites with flexural strength and toughness values (4 point bending) up to 470 MPa and 13 MPa-m$^{1/2}$, respectively [23].

## 5. Conclusions

A novel process has been used to fabricate dense, lightweight, ceramic-rich, ceramic/metal composites at a modest temperature with good control of shape and dimensions: the Displacive Compensation of Porosity (DCP) method. With the DCP method, the volume of ceramic consumed by a displacement reaction with a liquid metal is less than the volume of ceramic generated, so that composites with relatively high ceramic contents can be produced. The feasibility of producing ceramic-rich, ceramic/metal composites by the DCP method was demonstrated in the present work by fabricating MgO/Mg-Al composites from porous $Al_2O_3$. Molten magnesium was allowed to undergo pressureless infiltration into and reaction with rigid, porous alumina preforms at 1000 °C. By varying the relative density of the $Al_2O_3$ preforms, the oxide content of the resulting MgO/Mg-Al composites was adjusted from 70.4–85.6 vol %. The experimentally-measured values of MgO content and mass of the MgO/Mg-Al composites were in good agreement with values calculated from equations derived from the conservation of mass and volume. Bar-shaped MgO/Mg-Al composites that possessed relative densities of 97.7–99.9% and that retained the shapes and dimensions (to within 1.6%) of the starting alumina preforms were fabricated within 7.2 ks at 1000 °C. These bar-shaped MgO/Mg-Al composites possessed average flexural strength and toughness values of 244 MPa and 5.4 MPa $\cdot$ m$^{1/2}$, respectively, and exhibited excellent resistance to hydration.


## Acknowledgements

The financial support of the U.S. Air Force Office of Scientific Research under Grant No. F49620-95-1-0372 is gratefully acknowledged.


## References


1. M. C. BRESLIN, US Patent no. 5214011 May 25, (1993).
2. M. C. BRESLIN, J. RINGNALDA, L. XU, M. FULLER, J. SEEGER, G. S. DAEHN, T. OTANI and H. L. FRASER, *Mater. Sci. Eng. A* **A195** (1995) 113.
3. N. CLAUSSEN, D. E. GARCIA and R. JANSSEN, *J. Mater. Res.* **11** (1996) 2884.
4. S. SCHICKER, D. E. GARCIA, J. BRUHN, R. JANSSEN and N. CLAUSSEN, *J. Amer. Ceram. Soc.* **80** (1997) 2294.
5. *Idem., ibid.* **80** (1997) 2248.
6. W. G. FAHRENHOLTZ, K. E. EWSUK, R. E. LOEHMAN and A. P. TOMSIA, *Met. Mater. Trans. A* **27A** (1996) 2100.
7. K. G. EWSUK, S. J. GLASS, R. E. LOEHMAN, A. P. TOMSIA and W. G. FAHRENHOLTZ, *ibid.* **27A** (1996) 2122.
8. R. E. LOEHMAN, K. EWSUK and A. P. TOMSIA, *J. Amer. Ceram. Soc.* **79** (1996) 27.
9. W. G. FAHRENHOLTZ, K. G. EWSUK, D. T. ELLERBY and R. E. LOEHMAN, *ibid.* **79** (1996) 2497.
10. E. SAIZ, A. P. TOMSIA, R. E. LOEHMAN and K. EWSUK, *J. Euro. Ceram. Soc.* **16** (1996) 275.
11. JCPDS Cards No. 35-821 for Mg, 4-787 for Al, 1-1128 for $Al_{12}Mg_{17}$, 45-946 for MgO, 43-1484 for $Al_2O_3$, 21-1152 for $MgAl_2O_4$, 15-776 for $Al_6Si_2O_{13}$, 21-1276 for $TiO_2$ (rutile), 41-258 for $Al_2TiO_5$, 4-835 for NiO, 10-339 for $NiAl_2O_4$, 37-1484 for $ZrO_2$ (monoclinic), 19-629 for $Fe_3O_4$, and 43-1042 for $Nb_2O_5$.
12. P. KUMAR and K. H. SANDHAGE, US Patent Application no. *60/083, 534* April 29. (1998).
13. *Idem., J. Mater. Res.* **13** (1998) 3423.
14. J. L. MURRAY, *Bull. Alloy Phase Diag.* **3** (1982) 60.
15. J. B. WACHTMAN, "Mechanical Properties of Ceramics" (John Wiley & Sons, New York, 1996) p. 26.
16. "Metals Handbook," 9th ed. Vol. 2 (ASM International, Metals Park, OH, USA) p. 553.
17. I. BARIN, "Thermochemical Data of Pure Substances" (VCH Verlagsgesellschaft, Weinheim, Germany, 1989).
18. "Binary Alloy Phase Diagrams," Vols. 1 and 2, edited by T. B. Massalski, H. Okamoto, P. R. Subramanian and L. Kacprzak (American Society for Metals, Metals Park, OH, 1986) pp. 147, 1722.
19. "1998 Annual Book of ASTM Standards," Vol. 15.01 (American Society for Testing and Materials, W. Conshohocken, PA, 1998) pp. 88, 304.
20. B. R. LAWN, A. G. EVANS and D. B. MARSHALL, *J. Amer. Ceram. Soc.* **63** (1980) 574.
21. H. JYNGE and K. MOTZFELDT, *Electrochim. Acta* **25** (1980) 139.
22. W. P. TAI, T. WATARI and T. TORIKAI, *Ceram. Bull.* **76** (1997) 86.
23. K. A. ROGERS, P. KUMAR, R. CITAK, K. H. SANDHAGE, *J. Am. Ceram. Soc.* **82** (1999) 757.



*Received 25 November 1998*
*and accepted 4 May 1999*